# Benefits of cryopreservation as long-term storage method of encapsulated cardiosphere-derived cells for cardiac therapy: A biomechanical analysis

Laura Paz-Artigas [a,b], Kaoutar Ziani [c,d], Clara Alcaine [a,b], Claudia Báez-Díaz [e,f], Virginia Blanco-Blázquez [e,f], Jose Luis Pedraz [c,d,g], Ignacio Ochoa [a,b,d,*], Jesús Ciriza [a,b,d,*]

[a] Tissue Microenvironment (TME) Lab. Aragón Institute of Engineering Research (I3A), University of Zaragoza, Zaragoza, Spain
[b] Institute for Health Research Aragón (IIS Aragón), Zaragoza, Spain
[c] NanoBioCel Group, Laboratory of Pharmacy and Pharmaceutical Technology, Faculty of Pharmacy, University of the Basque Country UPV/EHU, Vitoria-Gasteiz 01006, Spain
[d] Biomedical Research Networking Center in Bioengineering, Biomaterials, and Nanomedicine, CIBER-BBN, Spain
[e] Jesús Usón Minimally Invasive Surgery Centre, Cáceres, Spain
[f] Centro de Investigación Biomédica en Red de Enfermedades Cardiovasculares (CIBER CV), Spain
[g] Bioaraba, NanoBioCel Research Group, Vitoria-Gasteiz, Spain

## ARTICLE INFO

## ABSTRACT

Cardiosphere-derived cells (CDCs) encapsulated within alginate-poly-L-lysine-alginate (APA) microcapsules present a promising treatment alternative for myocardial infarction. However, clinical translatability of encapsulated CDCs requires robust long-term preservation of microcapsule and cell stability, since cell culture at 37 °C for long periods prior to patient implantation involve high resource, space and manpower costs, sometimes unaffordable for clinical facilities. Cryopreservation in liquid nitrogen is a well-established procedure to easily store cells with good recovery rate, but its effects on encapsulated cells are understudied. In this work, we assess both the biological response of CDCs and the mechanical stability of microcapsules after long-term (i.e., 60 days) cryopreservation and compare them to encapsulated CDCs cultured at 37 °C. We investigate for the first time the effects of cryopreservation on stiffness and topographical features of microcapsules for cell therapy. Our results show that functionality of encapsulated CDCs is optimum during 7 days at 37 °C, while cryopreservation seems to better guarantee the stability of both CDCs and APA microcapsules properties during longer storage than 15 days. These results point out cryopreservation as a suitable technique for long-term storage of encapsulated cells to be translated from the bench to the clinic.

## 1. Introduction

Cell-based regenerative therapies are emerging as a promising strategy for the treatment of myocardial infarction (Ghiroldi et al., 2018; Tompkins et al., 2018). Among them, the use of cardiosphere-derived cells (CDCs) which produce growth factors involved in myocardial regeneration (Chimenti et al., 2010), has shown promising results in both preclinical and clinical trials (Makkar et al., 2012; Yee et al., 2014). Delivery of CDCs, or its secretions, reduces fibrotic scar size and mitigates microvascular obstruction, adverse remodelling and ventricular dilatation; improving myocardium viability and general cardiac function in porcine models of ischemic cardiomyopathy and myocardial infarction (Gallet et al., 2017; Kanazawa et al., 2015; Yee et al., 2014).

Despite successful CDCs delivery without host immunological response to graft (Blázquez et al., 2016), heartbeat motions typically result in continuous mechanical displacement of CDCs, thereby compromising the survival and engraftment rate of transplanted cells (Van Ramshorst et al., 2011).

CDCs microencapsulation is an interesting strategy to improve cell engraftment. Microencapsulation of therapeutic cells aims to preserve cells within a biocompatible hydrogel that allows exchange of nutrients and cell therapeutic products via diffusion, while avoiding foreign immune recognition (Farina et al., 2019; Lim and Sun, 1980). In myocardial infarction treatments, the bigger size of microcapsules, compared with individual cells, prevents microcapsule washout from myocardium into the bloodstream caused by the cardiac contractile forces (Al Kindi

et al., 2011; Paul et al., 2009). The success of microencapsulation for cell therapy requires an adequate microenvironment for encapsulated cell viability and compound diffusion, and a stable, biocompatible and non-immunogenic polymer surface. Suitable mechanical resistance is also desirable to prevent breakage and release of microcapsule contents (Ciriza et al., 2018; Orive et al., 2004; Rokstad et al., 2014). Alginate is a commonly used hydrogel in microencapsulation due to its excellent biocompatibility and low toxicity (Lee and Mooney, 2012; Zimmermann et al., 2007). To improve the stiffness of alginate-based microcapsules while maintaining low immunogenicity, microcapsules are subsequently coated with poly-L-lysine (PLL) and alginate (Orive et al., 2002; Virumbrales-Muñoz et al., 2021). The resulting microcapsule, known as alginate-PLL-alginate (APA) microcapsule, has been previously used to encapsulate CDCs, without affecting their viability and growth factor secretory capacity (Ziani et al., 2021).

Although microencapsulation may significantly improve cell therapy effectiveness, hospitals and clinical facilities lack equipment and expertise to encapsulate cells. Therefore, clinical translation requires a robust long-term storage that preserves microcapsule structure and cell stability. Maintenance of therapeutic cells for long periods of time at 37 °C incurs in high resource and manpower investments and can decrease the therapeutic abilities of cells overtime. Cryopreservation in liquid nitrogen is a well-established and easy procedure to store cells with good recovery rates. Although CDCs have been cryopreserved without altering their stem characteristics (Dutton et al., 2018), the effects of cryopreservation on encapsulated CDCs have not been reported yet.

Most research in microencapsulation has focused on the effects of freezing on cells behaviour (Gurruchaga et al., 2018), without addressing structural alterations of the microcapsules. However, microcapsule topographical and mechanical properties are key factors to ensure the effectiveness of microencapsulated implants. Characterization of these features *in vitro* can accelerate research, reducing validation prior to *in vivo* testing. Atomic Force Microscopy (AFM) is a powerful set of techniques to characterize surface properties. AFM is ideally suited to characterize microcapsule surface properties, since it provides nanometric resolution in physiologically relevant liquid media, and does not require significant sample preparation procedures that may impact microcapsule structure (Allison et al., 2010; Binnig et al., 1986; Lekka et al., 2004). Force spectroscopy-based measurements via AFM can provide both topographic and stiffness data of the microcapsule surface (Virumbrales-Muñoz et al., 2019). However, the small penetration ranges of AFM indentation, usually in the nanoscale, falls short in determining microcapsule overall stiffness. Large deformation assays, such as micromanipulation, aspiration, or microcapsule constriction, have been reported to measure whole microcapsule stiffness (Campillo et al., 2007; Kim et al., 2010; Le Goff et al., 2017; Neubauer et al., 2014). Therefore, combining AFM measurements with large deformation assays can provide a valuable overview of the most relevant microcapsule mechanical properties. In previous work, we applied for the first time an innovative workflow combining AFM Force Spectroscopy measurements with a custom-made constriction test to assess the mechanical properties of alginate-based microcapsules, (Virumbrales-Muñoz et al., 2021).

In this manuscript, we study the long-term endurance of cultured and cryopreserved microencapsulated CDCs, assessing both the biological response of CDCs and the mechanical integrity of cultured and cryopreserved microcapsules after 30 and 60 days, respectively. CDCs viability, metabolic activity and VEGF release were quantified and microcapsule integrity was investigated by combining force spectroscopy-based AFM measurements of the surface and a constriction assay.

## 2. Materials and methods

### 2.1. Cell culture

Cardiosphere derived cells (CDCs) were obtained from cardiac tissue explants of pigs. Tissue explants were subjected to enzymatic digestions and cultured. After three weeks, fibroblast-like cells migrating from the explant were seeded and cell clusters (i.e., cardiospheres) were formed. Cells migrating from these clusters (CDCs), were selected and expanded in standard cell culture flasks.

CDCs were cultured in complete medium composed of 65% Dulbecco's Modified Eagle's Medium (DMEM) Ham's F12 with 3.996 mM Ultra Glutamine (Lonza, Switzerland) and 35% Iscove's Modified Dulbecco's Medium (IMDM) (Lonza, Switzerland) supplemented with 10% FBS (Lonza, Switzerland), 1% Penicillin-Streptomycin (Lonza, Switzerland), 2 mM L-glutamine (Invitrogen), and 0.1 mM 2-mercaptoethanol (Sigma Aldrich, United States). Cells were maintained at 37 °C in a humidified 5% $CO_2$ atmosphere, and passaged every 2–3 days.

### 2.2. Cell encapsulation

Encapsulation was performed at room temperature, under aseptic conditions. UltraPure Low Viscosity High Guluronic, UPLVG, alginate (FMC Biopolymer, Norway) was resuspended in distilled water with 1% mannitol (Sigma Aldrich, Madrid, Spain) to obtain 1.5% (w/v) alginate and 0.1% alginate solutions. Final solutions were filtered through a 0.22 μm syringe filter (Millipore, MA, USA). Then, CDCs were suspended in the 1.5% alginate solution, at a concentration of $5 \times 10^6$ cells/mL, and extruded with a peristaltic pump (flow rate: 5.9 mL/h) through an electrostatic atomization generator VARV1 (Nisco, Switzerland).

The resulting alginate microcapsules were maintained in agitation for 15 min in a 55 mM $CaCl_2$ solution (Sigma Aldrich, Madrid, Spain) for complete ionic gelation. Afterwards, they were coated with 0.05 % (w/v) Poly-L-lysine, PLL (Sigma Aldrich, Madrid, Spain), by incubating with agitation during 5 min, followed by another coating step with 0.1% alginate for 5 min. The resulting microcapsules were divided in two groups. One group was maintained with complete medium at 37 °C, in a humidified 5% $CO_2$ and 95% air atmosphere standard incubator, and was tested at 1, 7, 15 and 30 days after production. The second group was maintained with complete medium and 10% of DMSO at −196 °C in liquid nitrogen and thawed at days 15, 30 and 60 after production. Thawed microcapsules were incubated for 24 h before testing.

### 2.3. Microcapsule cryopreservation

Microcapsules were stored in freshly prepared complete medium with 10% DMSO (ATCC), hereafter called cryoprotective solution. 200 μL of microcapsules containing CDCs were resuspended in cryovials (Nalgene) with 1 mL of the cryoprotective solution previously prepared. Cryovials were frozen at − 80 °C for one day on a Nalgene Cryo container and stored in liquid nitrogen tanks the following day. After 15, 30 and 60 days, cryovials were completely thawed by immersion in a 37 °C bath. Cryopreserved microcapsules were rinsed three times with 10 mL of complete medium to remove the remaining cryoprotectant solution and incubated for 24 h before testing.

### 2.4. Metabolic activity assay

Metabolic activity was determined with the Cell Counting Kit-8, CCK-8 (SigmaAldrich, United States), per manufacturer's instructions. 25 μL of microcapsule solution was rinsed, resuspended into 500 μL of culture medium supplemented with 50 μL of CCK-8 reagent, and plated in 5 wells of a 96-well plate. After incubation for 4 h at 37 °C, absorbance was measured on an Infinite M200 TECAN plate reader (TECAN Trading AG, Switzerland) at 450 nm and corrected at 650 nm. At least three independent experiments were analyzed for each day.

### 2.5. VEGF quantification

To quantify VEGF secretion, 500 μL of microcapsule supernatant were collected and stored at −80 °C for subsequent processing. Levels of VEGF within the supernatants were determined with VEGF ELISA Kit (My BioSource, Inc.), per manufacturer's instructions. Absorbance was measured at 450 nm on an Infinite M200 TECAN plate reader (TECAN Trading AG, Switzerland) and VEGF concentration was calculated from a standard curve. We performed at least three independent experiments, with three technical replicates per condition.

### 2.6. Cell viability

Microencapsulated cell viability was assessed after calcein AM/ethidium homodimer staining. Briefly, 50 μL of microcapsules were rinsed three times in DPBS (Gibco, United States) and resuspended in 500 μL of 0.5 μM ethidium homodimer-1 (Life Technologies, United States) and 0.5 μM calcein AM (Life Technologies, United States) solution. The samples were incubated in 24-well-plates for 45 min at room temperature, protected from light. Samples were observed under a Nikon Eclipse TE2000-S confocal microscope at 470 nm wavelength for calcein AM and 575 nm wavelength for ethidium homodimer staining. Random images were analyzed with the NIS Elements AR software, version 4.51.00. At least three independent experiments were performed for each condition.

### 2.7. Microcapsule constriction assay

Global microcapsule stiffness was determined using a custom-made constriction system described previously (Virumbrales-Muñoz et al., 2021). Briefly, measurements were performed within a methacrylate microfluidic device designed by BeOnChip S.L. (Spain) and manufactured by Aitiip Centro Tecnológico (Spain). This microdevice consisted of a Ø 400 μm tubular channel, sharply reduced to Ø 200 μm. A 1/16″ OD PTFE (Elveflow, France) and a TYGON (Saint-Gobain, ACF00002-C) tubing system were used to connect the microdevice to a pressure controller (OB1 Microfluidic Flow Control System, Elveflow). Optical inspection of the microfluidic channel was performed by an optical inverted microscope (Leica DMi8).

#### 2.7.1. Constriction measurements

The constriction system was perfused with culture media or DPBS. Microcapsules diluted in culture media were individually isolated in a U-shape 96-well plate (Sarstedt) for optical microscopy inspection (Nikon-Eclipse Ti-E). After measuring microcapsule diameter with NIS Elements Analysis Software (Nikon), each microcapsule was captured with a micropipette and injected into the system. Pressure lower than 1000 Pa was applied to place the microcapsule at the entrance of the microchannel constriction. Then, the pressure was increased at a constant rate of 100 Pa/s, pushing the microcapsule through the constriction. The microscopic optical image of the microdevice and the pressure measurements were video recorded during the whole process for posterior analysis. At least 10 microcapsules per condition were tested.

#### 2.7.2. Stiffness calculation from constriction data

The stiffness of microcapsules was determined as a pressure/deformation relationship ($\Delta P/\Delta \delta$). To obtain this relationship, videos of the constriction assay were processed using VLC media player software. After each 10-mbar pressure increment, the corresponding video frame was exported as an image file. The length occupied by the microcapsule in the Ø 200 μm channel was measured for each exerted pressure (ImageJ software) and normalized by the initial microcapsule diameter to calculate deformation. For small deformations, experimental results could be fitted to a linear curve from which the pressure/deformation relationship was obtained.

### 2.8. AFM measurements

Topographical and mechanical measurements of the microcapsule surface were performed by an AFM Nanowizard 3 system (JPK Instruments, Germany) mounted on an optical inverted microscope (Nikon-Eclipse).

#### 2.8.1. Tip calibration

AFM measurements were performed with qpBioAC-CI probes (NanoANdMore GMBH). The pyramidal shape of these probes' tips makes them suitable for high resolution imagining. Tip CB1 was chosen due to the adequacy of its nominal spring constant (0.3 N·m$^{-1}$) for samples in the kPa scale, such as APA microcapsule formulation (Virumbrales-Muñoz et al., 2019). The experimental spring constant of each new tip used was characterized by the Thermal Noise Method before performing any measurements (Hutter and Bechhoefer, 1993).

#### 2.8.2. Microcapsules sample preparation

Microcapsules were immobilized within a Ø 330 nylon mesh (Labopolis S.L.) to perform the AFM measurements in liquid. Mesh was glued in a Petri Dish (TPP Techno Plastic Products AG, 93040) using a standard 2-component cyanoacrylate adhesive. Then, the Petri Dish was filled with culture media, and bubbles lodged within the mess were dislodged via repeated pipetting. The dish was placed on the Petri-DishHeater (JPK Instruments, Germany) stage to reach a stable temperature of 37 °C. A sterile aliquot of microcapsules suspended in culture media was added to the Petri Dish, allowing microcapsules to sediment and locate within the mesh openings.

#### 2.8.3. Force spectroscopy measurements

Force spectroscopy-based images were acquired using the AFM Quantitative Imagining (QI) mode, as previously described (Virumbrales-Muñoz et al., 2019). Briefly, the calibrated cantilever was positioned over a mesh-immobilized microcapsule. High Z-lengths (2 μm), slow speeds (10 μm·s − 1) and low resolution (8x8 pixel size) were used to obtain the initial QI maps. Once stable measurements with a high signal/noise ratio were achieved, parameters were optimized for quicker (120 μm·s − 1) high resolution (256x256 pixel) imaging. Z-length was decreased to the nm scale to minimize sample drift effects during the acquisition but programmed to at least double the image height. For each microcapsule, two high resolution maps of 9 μm$^2$ and one high resolution map of 100 μm$^2$ were acquired. At least 10 microcapsules per condition were analyzed.

#### 2.8.4. AFM image processing

QI maps (golden color scale) were processed by DP software (JPK Instruments, Germany). From each map, a height image was extracted. Raw images were flattened by fitting to a second order polynomial line, to highlight small features in the overall curved surface. Then, a small degree of smoothing was applied to render pixel transition less evident.

#### 2.8.5. Young's Moduli extraction

Force spectroscopy curves, acquired as pixels of the QI maps, were processed by DP Software (JPK Instruments, Germany) to obtain Young's Moduli. Curves were fitted to a Hertz model modified for paraboloid indentors (JPK Instruments, 2008). Calculated values were shown as a blue color scale map.

#### 2.8.6. Bidimensional statistics

Topographical images were analyzed with Gwyddion open-source software to calculate bidimensional statistical parameters (i.e., Maximum Image Height, RMS, Ra, Skewness index and Kurtosis index) (Nečas and Klapetek, 2012).
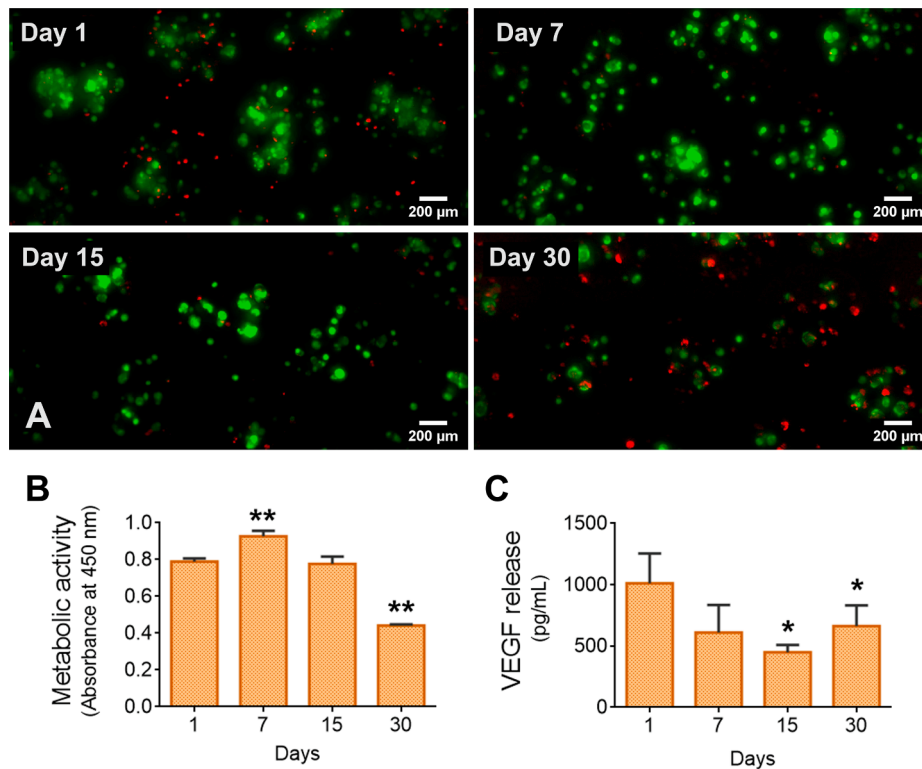
**Fig. 1.** Biochemical profile of encapsulated Cardiosphere-Derived-Cells (CDCs) cultured at 37 °C over a month. (A) Optical images of life-death assay, where alive cells were stained with calcein AM (green) and dead cells were stained with ethidium homodimer (red). (B) Metabolic activity of CDCs via CCK-8 assay. (C) Release profile of VEGF. Bars represent mean ± SD. **: $p < 0.01$ and *: $p < 0.05$ compared to day 1.

### 2.9. Statistical analysis

GraphPad Prism 6 software was used for the statistical analysis of all parameters. Data were expressed as mean ± standard deviation. Statistically significant differences were determined using ANOVA, Post Hoc Dunnett's multiple comparison test when data followed a normal distribution and Mann Whitney test for non-Gaussian data. Normal distribution was determined by Shapiro-Wilk normality test.
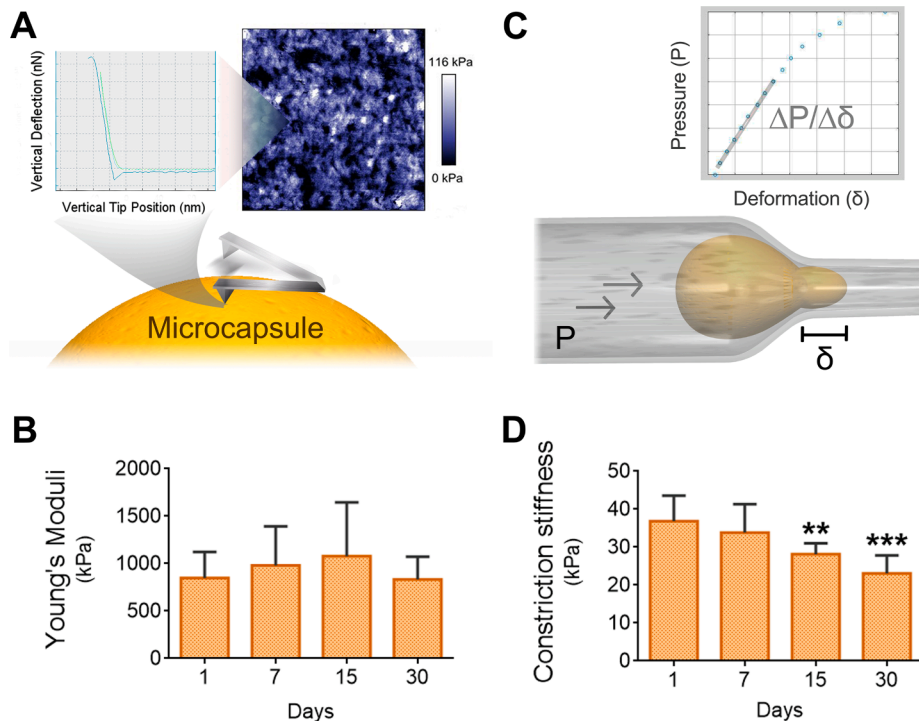


**Fig. 2.** Stiffness determination of Alginate-Poly-L-lysine-Alginate (APA) microcapsules loaded with Cardiosphere-Derived-Cells (CDCs) cultured at 37 °C for 30 days. (A) Graphic representation of the Atomic Force Microscopy (AFM) determination of microcapsules Young Modulus. Force-spectroscopy curves were acquired by indentation over the microcapsule surface and processed to obtain stiffness maps. (B) Average values of Young Modulus obtained from AFM stiffness maps. (C) Schematic representation of the constriction assay. Microcapsules were subjected to an increasing pressure, P, and forced to penetrate within a narrow microfluidic channel. Pressure data was then plotted against deformation, δ. For small penetrations, the pressure/deformation ratio remained constant. (D) Stiffness calculated as pressure/deformation ratio from constriction assay. Bars represent mean ± SD. n = at least 10 microcapsules. ***: $p < 0.001$ and **: $p < 0.01$ compared to day 1.
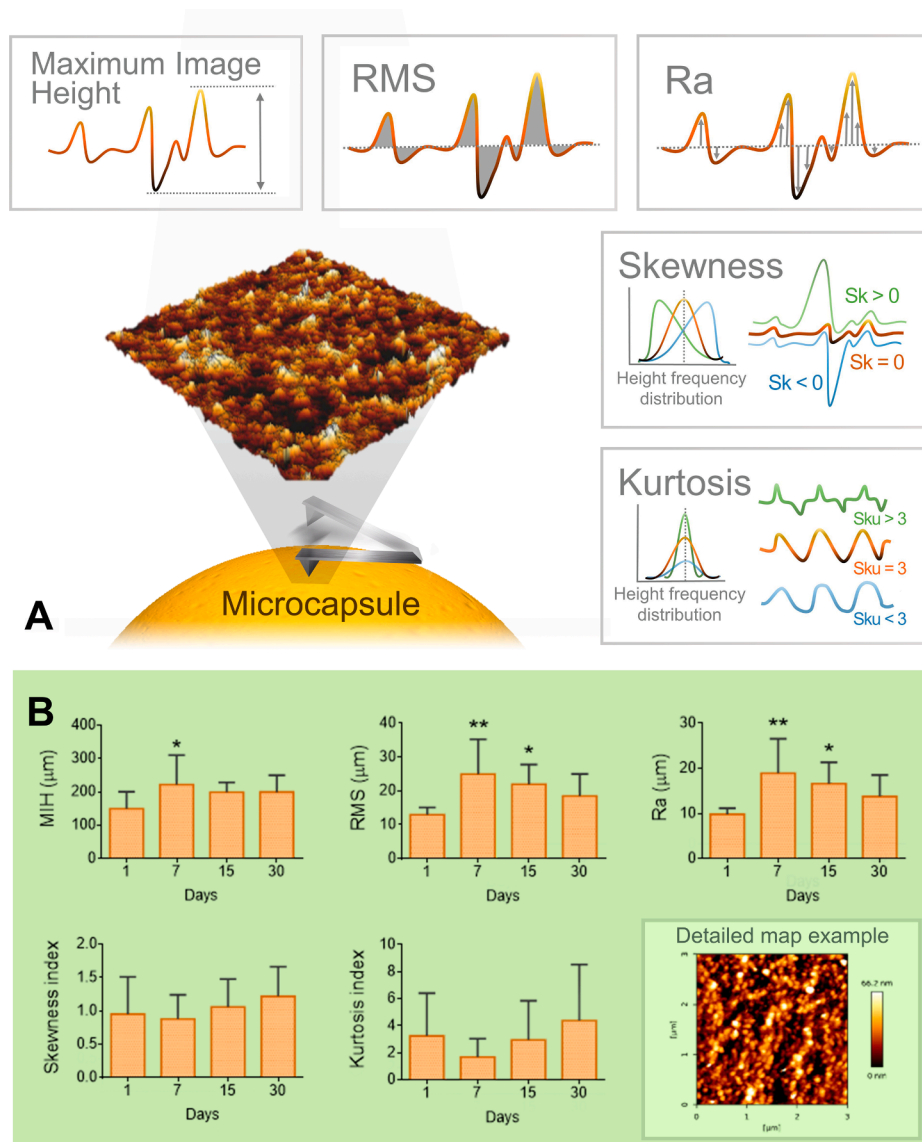
**Fig. 3.** Topographical analysis of the microcapsule surface via Atomic Force Microscopy (AFM) performed. (A) Topography images of the microcapsule surface were acquired by AFM and characterized with standard topography parameters: Maximum Image Height (MIH), RMS roughness, Ra roughness, Skewness index and Kurtosis index. The example line profiles illustrate the physical significance of each parameter. Skewness and Kurtosis index are dependent on height frequency distribution. (B) Standard topography parameters determined from 9 μm2 detailed images. Bars show mean ± SD. n = at least 10 microcapsules. **: $p < 0.01$ and *: $p < 0.05$ compared to day 1.

## 3. Results and discussion

### 3.1. Encapsulated CDCs in culture have lower viability and VEGF release overtime

We investigated the effects of long-term culture on encapsulated cardiosphere-derived cells (CDCs) (Ziani et al., 2021). To this end, CDCs were immobilized within spherical alginate-based gels double coated with poly-L-lysine and alginate. We used ultrapure low viscosity and high guluronic alginate, since animal implantation of high purity alginate gels do not to induce significant foreign body reaction (Lee and Lee, 2009; Orive et al., 2002). Resulting microcapsules, known as alginate-poly-L-lysine-alginate (APA) microcapsules, presented an average size of 420 μm (Supplemental Fig. 1) and were incubated in culture media at 37 °C for 30 days.

Cell viability (Fig. 1A) improved during the first 7 days after encapsulation, suggesting an adaptation process to the hydrogel matrix microenvironment, as reported for other cell types, such as MSCs (Ciriza et al., 2018; Ziani et al., 2021). However, a certain cell death, already detected at day 15, became evident 30 days after encapsulation, as shown by fluorescence microscopy images of encapsulated CDCs stained with calcein/ethidium homodimer. Similarly, metabolic activity

(Fig. 1B) inverted its initial tendency at day 15 and continued decreasing to almost half its initial value after 30 days of culture, as measured via CCK8-based assay. We next assessed the regenerative potential of encapsulated CDCs by quantifying VEGF release (Fig. 1C), which also showed a significant reduction from 15 days forward. While a high cell growth would be counterproductive since it can lead to microcapsule breakage (Orive et al., 2003), the cell progressive deterioration after 15 days of culture at 37 °C warns against long-term storage of encapsulated CDCs at this *in vitro* culture conditions.

### 3.2. Microcapsule core of encapsulated CDCs suffers alterations over time at 37°, while surface topography and stiffness remain unchanged

It is well known that stiffness and mechanical stability of scaffolds have a great impact on cells performance in 3D cultures (Breuls et al., 2008; Mason et al., 2013; Petersen et al., 2012; Sasikumar et al., 2019). In fact, CDCs maturation has been proved to depend on scaffold stiffness (Xu et al., 2014). Therefore, we investigated whether the observed CDCs viability, metabolic activity and VEGF release profiles were related to microcapsules mechanical stability. Force Spectroscopy via Atomic Force Microscopy (AFM) allows the fine determination of hydrogels and soft materials Young's Modulus (Garcia, 2020; Giménez et al., 2017) and

has been used for microcapsules mechanical characterization in physiological conditions (in liquid at 37 °C) (Chui et al., 2019; Ciriza et al., 2015; Fery et al., 2004; Sarrazin et al., 2016; Virumbrales-Muñoz et al., 2021). Therefore, we scanned square areas of microcapsules surface (Fig. 2A) by AFM's tip indentation, obtaining force-spectroscopy curves that were fitted to the Hertz model and generating maps of the microcapsule surface stiffness. Young Modulus mean values obtained from these maps (Fig. 2B) did not change overtime for microcapsules incubated at 37 °C.

Since AFM is meant for the characterization of material surfaces, we complemented AFM measurements with a constriction assay test (Fig. 2C) previously reported by our group (Virumbrales-Muñoz et al., 2021). In this test microcapsules (diameter of 400 μm) are forced to cross through a narrow microfluidic channel (diameter of 200 μm), assessing the resistance of the microcapsule to large deformations, and therefore providing a macro mechanical measurement of stiffness. Determining the elastic modulus of microcapsules from large deformation assays is challenging, since a great range of strains and stresses are involved. To accurately report microcapsule elastic modulus from this assay, a complex and exhaustive simulation of the whole process (e.g., via finite elements) would be needed. However, since our goal is to investigate significant alterations of microcapsule stability through time, a simpler approach can be used to estimate microcapsule stiffness. As previously reported (Le Goff et al., 2017; Virumbrales-Muñoz et al., 2021), the pressure/deformation ratio, where deformation is represented by the

microcapsule penetration length inside the narrow channel, may serve as a reliable parameter to compare stiffness of different microcapsules. Microcapsule stiffness characterized via our constriction assay showed a constant decrease overtime with significant differences at day 15 of incubation, which became more evident after 30 days in culture at 37 °C (Fig. 2D). It must be noted that the constant obtained from this assay does not represent the elastic modulus and, thus, both stiffness measurements (Fig. 2B and D) should not be compared in terms of absolute values, but tendencies through time.

We previously observed that APA microcapsules show not only surface Young Modulus 30-fold higher than nude alginate microcapsules, but also 2-fold higher constriction stiffness (Virumbrales-Muñoz et al., 2021), therefore suggesting an important contribution of alginate-PLL double coating to the general stiffness characterized by constriction assay. Since surface Young Modulus remains unaltered after 30 days in cultured APA microcapsules, we can conclude that the observed time-dependent decrease in APA constriction stiffness is probably related to changes in the alginate core instead of the coating. Therefore, PLL coating would help keeping the shape and surface mechanical properties of microcapsules overtime. In fact, alginate-based microcapsules culture within saline medium has proved to cause degradation of their structure integrity, probably due to an ion exchange with $Ca^{2+}$ ions in the cross-linked alginate, which is not observed when microcapsules are preserved in free-ion water (Bajpai and Sharma, 2004; Hunt et al., 2010; LeRoux et al., 1999; Moya et al., 2012). Notably, viability, metabolic
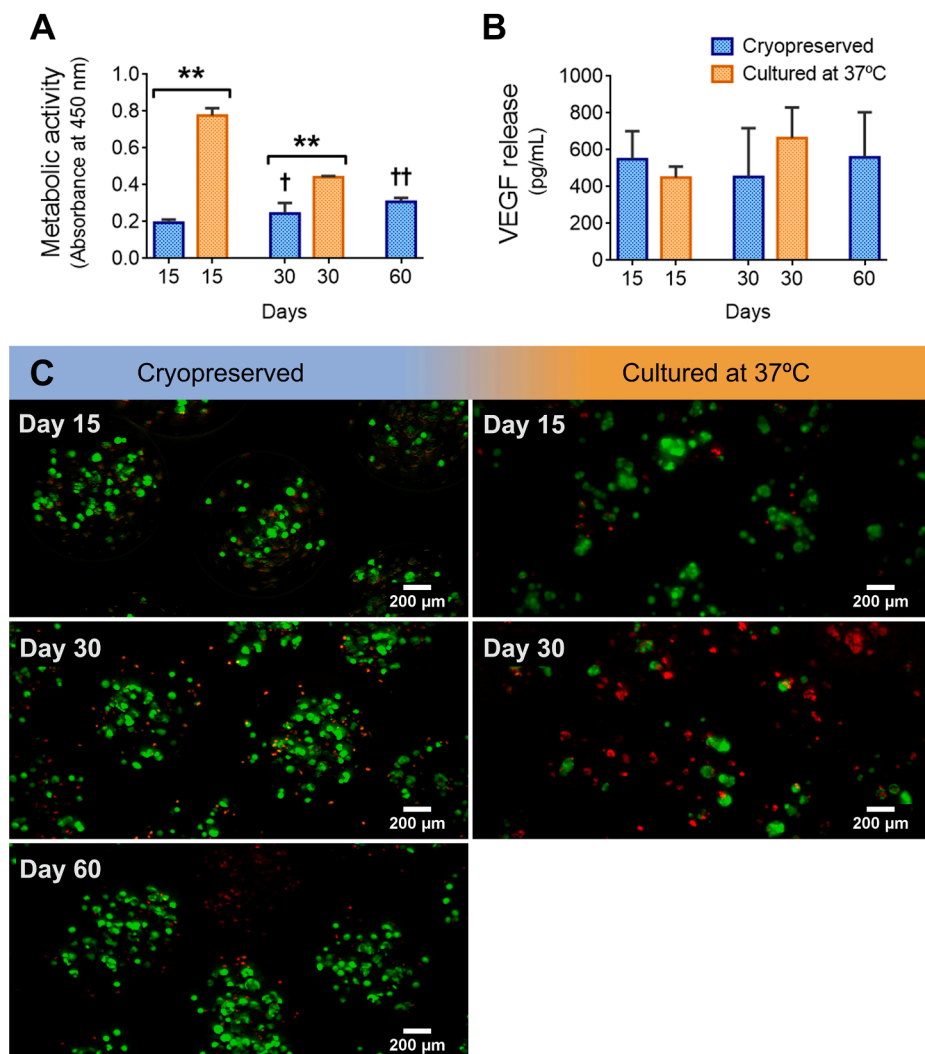


**Fig. 4.** Biochemical behaviour of encapsulated Cardiosphere-Derived-Cells (CDCs) after cryopreservation. Cells were frozen one day after encapsulation, thawed after their corresponding cryopreservation period and incubated at 37 °C in culture media 24 h before performing any assay. (A) Metabolic activity of CDCs via CCK-8 assay. (B) Release profile of Vascular Endothelial Growth Factor (VEGF). (C) Optical images of a life-death assay, where alive cells were stained with calcein (green) and dead cells were stained with ethidium homodimer (red). Bars show mean ± SD. ***: p < 0.001 comparing cryopreservation vs incubation at 37 °C. ††: p < 0.01 compared to day 15 of cryopreservation.
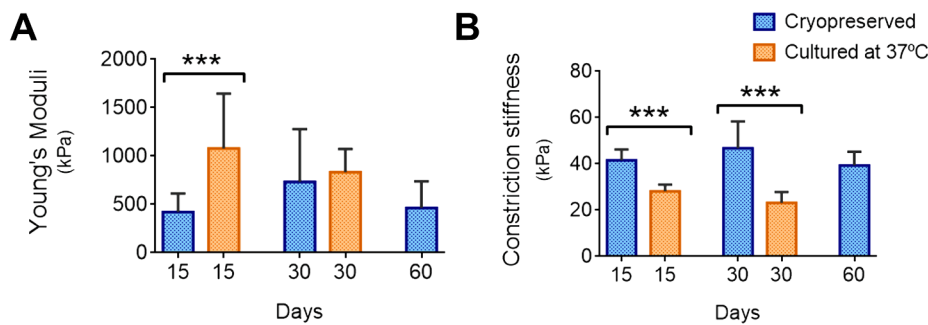
**Fig. 5.** Effect of cryopreservation on the stiffness of Alginate-Poly-L-lysine-Alginate (APA) microcapsules loaded with Cardiosphere-Derived-Cells (CDCs). (A) Microcapsule Young's Moduli obtained from force spectroscopy measurements via Atomic Force Microscopy (AFM). (B) Stiffness of microcapsule calculated as the pressure/deformation ratio from constriction assay. Bars represent mean ± SD. n = at least 10 microcapsules. ***: p < 0.001 comparing cryopreservation vs incubation at 37 °C.

activity and VEGF release of encapsulated CDCs presented a similar tendency to global microcapsule stiffness. These combined results suggest a relationship between the loss of integrity of the microcapsule core and the alterations of the cell's behaviour through time, while the double coating of the surface may remain unaltered.

Since the main purpose of cell encapsulation is concealing the therapeutic cells from the host immune surveillance, producing robust microcapsules that maintain a stable and non-immunogenic surface is key to therapy success. Thus, we pursued the characterization of microcapsule surfaces by investigating its topographical features through AFM (Fig. 3A). From each force-spectroscopy curve, the sample height was obtained and depicted as a pixel of a topographic map. We acquired large maps of 100 μm² (Supplemental Fig. 2) to verify the homogeneity of the microcapsule surfaces and detailed maps of 9 μm² (Fig. 3B) to increase the resolution of the topographical features. Classical parameters established by ISO standards (International Organisation of Standardization, 2012) for topography quantitative analysis of material surfaces are Maximum Image Height (MIH), RMS, Ra, Skewness index and Kurtosis index (Fig. 3A) (Bonyar, 2015; Duboust et al., 2017; Kundrak et al., 2008; Petrochenko et al., 2015). MIH represents the absolute distance between the highest peak and the lowest pore within the entire image. RMS and Ra parameters quantify surface deviation from a flat plane, determining surface roughness. Ra is calculated as the average distance that the surface deviates from the flat plane, while RMS is obtained from the area enclosed between these two elements. Surface asymmetry is determined by the Skewness index, with positive values when peaks emerge from an overall flat surface, and negative values when valleys are more prominent. Finally, the sharpness of peaks is calculated by the Kurtosis index, with high values of Kurtosis representing a very sharp surface and low values, rounded profiles. Detailed topography maps of CDCs-loaded microcapsules (Fig. 3B) showed a small increase of MIH at day 7, recovering initial values at day 15. Microcapsules presented similar roughness profiles in both Ra and RMS. After 7 days of incubation, surface roughness increased, reducing at day 15 and recovering initial values after 30 days, similar tendency than encapsulated CDCs viability and metabolic activity (Fig. 1). These variations in MIH and roughness could be related to CDCs growth and protrusion, since there is a relationship between cell growth and microcapsule roughness increase, without alteration of the surface roughness in empty capsules (Bhujbal et al., 2014). Regarding surface asymmetry, microcapsule surface remained with constant Skewness index during the whole period of incubation, with positive values, suggesting the predominance of peaks instead of a more porous surface. Similar to Skewness, no variations on Kurtosis index were detected overtime, indicating no changes on microcapsule surfaces peaks shape.

Overall, microcapsule surface remained stable after 30 days of incubation at 37 °C, characterized by the presence of peaks with slightly sharp shape, with an initial increase in roughness, which was progressively reduced, but not affecting neither the peak sharp shape, nor the local stiffness of the microcapsule surface. However, microcapsule global stiffness and encapsulated CDCs suffered alterations after 15 days of culture, which became more severe at day 30. Those tendencies

suggest that longer periods of incubation at 37 °C could render an ineffective therapy of encapsulated CDCs if grown at 37 °C patient implantation.

### 3.3. Microcapsule surface of encapsulated CDCs suffers slight alterations after 15 days on cryopreservation, while core remains stable

Cryopreservation is a well-established method for the long-term storage of cells and biological samples, reducing cost and facilitating the storage and transport of encapsulated cells from research laboratories to clinical facilities. In fact, the combination of classical cryoprotectors, such as DMSO, and cell immobilization within alginate or other hydrogel matrix has proven to enhance the cryoprotective effect in several cell types (Gurruchaga et al., 2018; Malpique et al., 2010; Matsumoto et al., 2001). However, to facilitate clinical implementation of cryopreserved encapsulated cells, viability and capsule stability should not be significantly affected by this procedure. As a framework for comparison, we used microcapsules incubated at 37 °C and compared the effects of culture at 37 °C versus cryopreservation on encapsulated CDCs properties at both 15 and 30 days. For cryopreservation, microcapsules were frozen 24 h after CDCs encapsulation, maintained in liquid nitrogen, thawed at the mentioned days, and kept in culture at 37 °C during another 24 h before inspection. Since cryopreservation is meant for long-term storage, we also analyzed the effects of 60 days of cryopreservation and compare it to shorter cryopreservation times.

Metabolic activity of encapsulated CDCs (Fig. 4A) after 15 days of cryopreservation plummeted compared to counterparts maintained at 37 °C. This decrease seemed to be related to the frozen process itself, as longer periods of cryopreservation were not translated to lower metabolic activity. Conversely, this parameter tended to improve with longer cryopreservation periods, being significantly higher after 60 days of cryopreservation, compared to 15 days. Moreover, at day 30 no significant differences were detected in metabolic activity between cultured and cryopreserved microcapsules. The tendency of metabolic activity suggested that better metabolic activities are achieved by cryopreserving than culturing in storage periods longer than 15 days. Quantifying the release of VEGF, no significant differences were detected among cryopreserved and cultured encapsulated CDCs overtime, remaining constant for 60 days (Fig. 4B). Similarly, cell viability was not affected by cryopreservation time (Fig. 4C). Therefore, we consider that although encapsulated CDCs viability is optimal during 7 days cultured at 37 °C, cryopreservation seems to better preserve cell properties at longer storage periods. In fact, non-encapsulated CDCs have previously been cryopreserved without significant changes in their stem profile (Dutton et al., 2018), in accordance with our data with encapsulated CDCs.

We next assessed the effects of cryopreservation on the mechanical stability of APA microcapsules. We determined both Young Modulus of microcapsule surface by means of AFM (Fig. 5A), and overall stiffness by constriction assay (Fig. 5B). The constriction assay revealed no changes in stiffness overtime for the cryopreserved capsules, with higher values than their counterparts at 37 °C. These results suggest that the degradation of alginate gel caused by the exchange of calcium ions that cross-
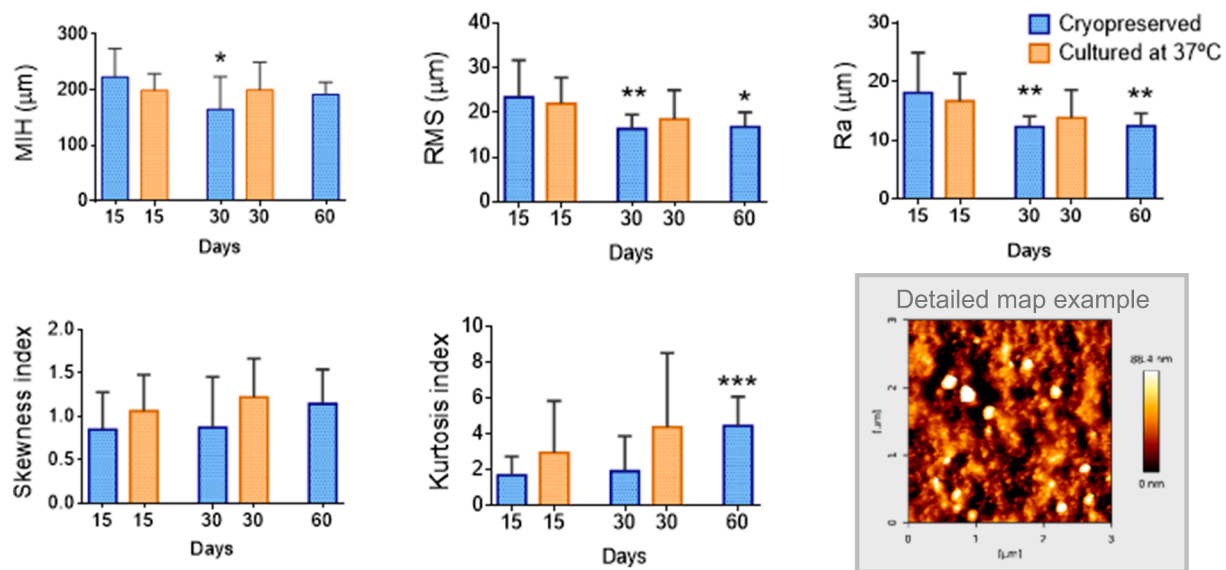
**Fig. 6.** Effect of cryopreservation on topographical features of Alginate-Poly-L-lysine-Alginate (APA) microcapsules loaded with Cardiosphere-Derived-Cells (CDCs). Detailed topography maps of the microcapsule surface were acquired by Atomic Force Microscopy (AFM) and characterized by determination of standard topography parameters: Maximum Image Height (MIH), RMS roughness, Ra roughness, Skewness index and Kurtosis index. Bars represent mean $\pm$ SD. n = at least 10 microcapsules. ***: $p < 0.001$, **: $p < 0.01$ and *: $p < 0.05$ compared to day 15 of cryopreservation.

link the structure with ions of the medium during culture is avoided when microcapsules are cryopreserved. While surface stiffness remained unchanged during incubation at 37 °C, cryopreservation reduced Young Modulus as determined by AFM, suggesting that freezing procedure affects microcapsule coating. However, when compared to its counterpart, no significant differences in Young's Moduli were detected after 30 days of cryopreservation. We can conclude that long term storage of encapsulated CDCs provides lower alteration of microcapsule mechanical stability than culture at 37 °C, with similar surface stiffness.

Regarding microcapsules topography (Fig. 6), cryopreservation had no significant effect on MIH compared to microcapsules culture at 37 °C. Similarly, the roughness of cryopreserved microcapsules determined by RMS and Ra showed no significant differences to their counterparts at 15 and 30 days. However, RMS and Ra data revealed surface roughness to have the opposite tendency on cryopreserved microcapsules than on cultured at 37 °C (Fig. 3), with a significant decrease when comparing days 30 and 60 to day 15 of cryopreservation, suggesting a smoothing of microcapsule surfaces caused by long-term cryopreservation. While no roughness increase caused by cell growth and protrusion is expected for cryopreserved microcapsules, the smoothing of the surface is harder to explain. APA microcapsules are known to have a relative smooth surface, since poly-L-lisine (PLL) single coating (AP microcapsules) (Virumbrales-Muñoz et al., 2019) or PLL and alginate double coating (APA microcapsules) (Virumbrales-Muñoz et al., 2021) have proved to reduce surface roughness of alginate microcapsules. An increase in smoothness can be achieved by adding a new coating of PEG-Amine (Chen et al., 1998). However, cryopreservation process is not expected to cause any chemical modification of the microcapsule coating. In PLL coated capsules, surface roughness is also reduced by chelation of the inner alginate hydrogel (Gattás-Asfura et al., 2014), but cryopreservation caused no alteration of the alginate core, as reported by constriction assay. To our knowledge, there are no studies on APA microcapsule degradation processes that could clarify the possible causes of the surface smoothing observed during cryopreservation of encapsulated CDCs. Finally, Skewness and Kurtosis indexes showed no significant differences between cultured and cryopreserved microcapsules at any time point of analysis. Only Kurtosis showed a significant increase after 60 days compared to 15 days of cryopreservation and, even so, this value was comparable to Kurtosis of microcapsules cultured at 37 °C during 30 days. Cryopreserved microcapsule surfaces kept the same tendency to

peaks and slightly sharp contours than their cultured counterparts.

In brief, mechanical analysis of CDCs-loaded APA microcapsules has shown that cryopreservation has no effect on the microcapsule core, while slightly reducing surface stiffness and roughness. Although further investigation may be necessary to characterize the physicochemical effects of cryopreservation on microcapsule surfaces, our results are promising, since a smooth surface of biomaterials has been related to low response after implantation (Bhujbal et al., 2014; Bünger et al., 2003; de Vos et al., 2006; Li et al., 2018).

## 4. Conclusions

We have investigated for the first time the mechanical alterations of cell-loaded microcapsules after cryopreservation, combining topographical and mechanical characterization of microcapsules. Our results show that functionality of encapsulated CDCs, as assessed via metabolic activity, viability and secretory capacity of cells, is optimum after 7 days of culture at 37 °C, maintaining topographical and mechanical properties of freshly produced microcapsules. However, cryopreservation seems to better guarantee the stability of both CDCs and APA microcapsules properties in long-term storage. While further investigation on *in vivo* effects of cryopreservation on microcapsules is necessary, such as microcapsule recognition by the immune system, our results predict a promising translation to clinics of cryopreservation for encapsulated CDCs therapy, which would reduce time and resources requirements for hospitals and health facilities.

## Declaration of Competing Interest

The authors declare that they have no known competing financial interests or personal relationships that could have appeared to influence the work reported in this paper.

### Research data

The data that support the findings of this study are available on request from the corresponding author.

## Appendix A. Supplementary data

Supplementary data to this article can be found online at https://doi.org/10.1016/j.ijpharm.2021.121014.

## References

Al Kindi, A.H., Asenjo, J.F., Ge, Y., Chen, G.Y., Bhathena, J., Chiu, R.-J., Prakash, S., Shum-Tim, D., 2011. Microencapsulation to reduce mechanical loss of microspheres: Implications in myocardial cell therapy. Eur. J. Cardio-thoracic Surg. 39 (2), 241–247. https://doi.org/10.1016/j.ejcts.2010.03.066.

Allison, D.P., Mortensen, N.P., Sullivan, C.J., Doktycz, M.J., 2010. Atomic force microscopy of biological samples. Wiley Interdiscip. Rev. Nanomedicine Nanobiotechnology. https://doi.org/10.1002/wnan.104.

Bajpai, S.K., Sharma, S., 2004. Investigation of swelling/degradation behaviour of alginate beads crosslinked with Ca2+ and Ba2+ ions. React. Funct. Polym. 59 (2), 129–140. https://doi.org/10.1016/j.reactfunctpolym.2004.01.002.

Bhujbal, S.V., De Haan, B., Niclou, S.P., De Vos, P., 2014. A novel multilayer immunoisolating encapsulation system overcoming protrusion of cells. Sci. Rep. 4, 1–8. https://doi.org/10.1038/srep06856.

Binnig, G., Quate, C.F., Gerber, C., 1986. Atomic force microscope. Phys. Rev. 56 (9), 930–933. https://doi.org/10.1103/PhysRevLett.56.930.

Blázquez, R., Sánchez-Margallo, F.M., Crisóstomo, V., Báez, C., Maestre, J., Álvarez, V., Casado, J.G., 2016. Intrapericardial delivery of cardiosphere-derived cells: An immunological study in a clinically relevant large animal model. PLoS One 11, e0149001. https://doi.org/10.1371/journal.pone.0149001.

Bonyar, A., 2015. Application of localization factor for the detection of tin oxidation with AFM, in: 2015 IEEE 21st International Symposium for Design and Technology in Electronic Packaging, SIITME 2015. Institute of Electrical and Electronics Engineers Inc., pp. 25–30. https://doi.org/10.1109/SIITME.2015.7342289.

Breuls, R.G.M., Jiya, T.U., Smit, T.H., 2008. Scaffold Stiffness Influences Cell Behavior: Opportunities for Skeletal Tissue Engineering. Open Orthop. J. 2 (1), 103–109. https://doi.org/10.2174/1874325000802010103.

Bünger, C.M., Gerlach, C., Freier, T., Schmitz, K.P., Pilz, M., Werner, C., Jonas, L., Schareck, W., Hopt, U.T., de Vos, P., 2003. Biocompatibility and surface structure of chemically modified immunoisolating alginate-PLL capsules. J. Biomed. Mater. Res. - Part A 67A (4), 1219–1227. https://doi.org/10.1002/jbm.a.v67a:410.1002/jbm.a.10094.

Campillo, C., Pépin-Donat, B., Viallat, A., 2007. Responsive viscoelastic giant lipid vesicles filled with a poly(N-isopropylacrylamide) artificial cytoskeleton. Soft Matter 3, 1421–1427. https://doi.org/10.1039/b710474j.

Chen, J.-P., Chu, I.-M., Shiao, M.-Y., Hsu, B.-S., Fu, S.-H., 1998. Microencapsulation of islets in PEG-amine modified alginate-poly(L-lysine)-alginate microcapsules for constructing bioartificial pancreas. J. Ferment. Bioeng. 86 (2), 185–190. https://doi.org/10.1016/S0922-338X(98)80059-7.

Chimenti, I., Smith, R.R., Li, T.-S., Gerstenblith, G., Messina, E., Giacomello, A., Marbán, E., 2010. Relative roles of direct regeneration versus paracrine effects of human cardiosphere-derived cells transplanted into infarcted mice. Circ. Res. 106 (5), 971–980. https://doi.org/10.1161/CIRCRESAHA.109.210682.

Chui, C.-Y., Bonilla-Brunner, A., Seifert, J., Contera, S., Ye, H., 2019. Atomic force microscopy-indentation demonstrates that alginate beads are mechanically stable under cell culture conditions. J. Mech. Behav. Biomed. Mater. 93, 61–69. https://doi.org/10.1016/j.jmbbm.2019.01.019.

Ciriza, J., Saenz del Burgo, L., Gurruchaga, H., Borras, F.E., Franquesa, M., Orive, G., Hernández, R.M., Pedraz, J.L., 2018. Graphene oxide enhances alginate encapsulated cells viability and functionality while not affecting the foreign body response. Drug Deliv 25 (1), 1147–1160. https://doi.org/10.1080/10717544.2018.1474966.

Ciriza, J., Saenz del Burgo, L., Virumbrales-Muñoz, M., Ochoa, I., Fernandez, L.J., Orive, G., Hernandez, R.M., Pedraz, J.L., 2015. Graphene oxide increases the viability of C2C12 myoblasts microencapsulated in alginate. Int. J. Pharm. 493 (1-2), 260–270. https://doi.org/10.1016/j.ijpharm.2015.07.062.

de Vos, P., Faas, M.M., Strand, B., Calafiore, R., 2006. Alginate-based microcapsules for immunoisolation of pancreatic islets. Biomaterials 27 (32), 5603–5617. https://doi.org/10.1016/j.biomaterials.2006.07.010.

Duboust, N., Ghadbeigi, H., Pinna, C., Ayvar-Soberanis, S., Collis, A., Scaife, R., Kerrigan, K., 2017. An optical method for measuring surface roughness of machined carbon fibre-reinforced plastic composites. J. Compos. Mater. 51 (3), 289–302. https://doi.org/10.1177/0021998316644849.

Dutton, L.C., Church, S.A.V., Hodgkiss-Geere, H., Catchpole, B., Huggins, A., Dudhia, J., Connolly, D.J., 2018. Cryopreservation of canine cardiosphere-derived cells: Implications for clinical application. Cytom. Part A 93, 115–124. https://doi.org/10.1002/cyto.a.23186.

Farina, M., Alexander, J.F., Thekkedath, U., Ferrari, M., Grattoni, A., 2019. Cell encapsulation: Overcoming barriers in cell transplantation in diabetes and beyond. Adv. Drug Deliv. Rev. 139, 92–115. https://doi.org/10.1016/j.addr.2018.04.018.

Fery, A., Dubreuil, F., Möhwald, H., 2004. Mechanics of artificial microcapsules. New J. Phys. 6, 18. https://doi.org/10.1088/1367-2630/6/1/018.

Gallet, R., Dawkins, J., Valle, J., Simsolo, E., De Couto, G., Middleton, R., Tseliou, E., Luthringer, D., Kreke, M., Smith, R.R., Marbán, L., Ghaleh, B., Marbán, E., 2017. Exosomes secreted by cardiosphere-derived cells reduce scarring, attenuate adverse remodelling, and improve function in acute and chronic porcine myocardial infarction. Eur. Heart J. 38, 201–211. https://doi.org/10.1093/eurheartj/ehw240.

Garcia, R., 2020. Nanomechanical mapping of soft materials with the atomic force microscope: Methods, theory and applications. Chem. Soc. Rev. 49 (16), 5850–5884. https://doi.org/10.1039/D0CS00318B.

Gattás-Asfura, K.M., Valdes, M., Celik, E., Stabler, C.L., 2014. Covalent layer-by-layer assembly of hyperbranched polymers on alginate microcapsules to impart stability and permselectivity. J. Mater. Chem. B 2 (46), 8208–8219. https://doi.org/10.1039/C4TB01241K.

Ghiroldi, A., Piccoli, M., Cirillo, F., Monasky, M., Ciconte, G., Pappone, C., Anastasia, L., 2018. Cell-based therapies for cardiac regeneration: A comprehensive review of past and ongoing strategies. Int. J. Mol. Sci. 19 (10), 3194. https://doi.org/10.3390/ijms19103194.

Giménez, A., Uriarte, J.J., Vieyra, J., Navajas, D., Alcaraz, J., 2017. Elastic properties of hydrogels and decellularized tissue sections used in mechanobiology studies probed by atomic force microscopy. Microsc. Res. Tech. https://doi.org/10.1002/jemt.22740.

Gurruchaga, H., Saenz del Burgo, L., Hernandez, R.M., Orive, G., Selden, C., Fuller, B., Ciriza, J., Pedraz, J.L., 2018. Advances in the slow freezing cryopreservation of microencapsulated cells. J. Control. Release. 281, 119–138. https://doi.org/10.1016/j.jconrel.2018.05.016.

Hunt, N.C., Smith, A.M., Gbureck, U., Shelton, R.M., Grover, L.M., 2010. Encapsulation of fibroblasts causes accelerated alginate hydrogel degradation. Acta Biomater. 6 (9), 3649–3656. https://doi.org/10.1016/j.actbio.2010.03.026.

Hutter, J.L., Bechhoefer, J., 1993. Erratum: Calibration of atomic-force microscope tips (Review of Scientific Instruments (1993) 64 (1868)). Rev. Sci. Instrum. doi 10 (1063/1), 1144449.

International Organisation of Standardization, 2012. ISO 25178-2:2012. Geom. Prod. Specif. – Surf. texture Areal - Part 2 Terms, Defin. Surf. texture parameters.

Instruments, J.P.K., 2008. Determining the elastic modulus of biological samples using atomic force microscopy. JPK Instruments Appl, Note.

Kanazawa, H., Tseliou, E., Malliaras, K., Yee, K., Dawkins, J.F., De Couto, G., Smith, R.R., Kreke, M., Seinfeld, J., Middleton, R.C., Gallet, R., Cheng, K.e., Luthringer, D., Valle, I., Chowdhury, S., Fukuda, K., Makkar, R.R., Marbán, L., Marbán, E., 2015. Cellular postconditioning: Allogeneic cardiosphere-derived cells reduce infarct size and attenuate microvascular obstruction when administered after reperfusion in pigs with acute myocardial infarction. Circ. Hear. Fail. 8 (2), 322–332. https://doi.org/10.1161/CIRCHEARTFAILURE.114.001484.

Kim, K., Cheng, J.i., Liu, Q., Wu, X.Y., Sun, Y.u., 2010. Investigation of mechanical properties of soft hydrogel microcapsules in relation to protein delivery using a MEMS force sensor. J. Biomed. Mater. Res. - Part A 92A (1), 103–113. https://doi.org/10.1002/jbm.a.v92a:110.1002/jbm.a.32338.

Kundrak, J., Gyani, K., Bana, V., 2008. Roughness of ground and hard-turned surfaces on the basis of 3D parameters. Int. J. Adv. Manuf. Technol. 38 (1-2), 110–119. https://doi.org/10.1007/s00170-007-1086-9.

Le Goff, A., Kaoui, B., Kurzawa, G., Haszon, B., Salsac, A.-V., 2017. Squeezing bio-capsules into a constriction: Deformation till break-up. Soft Matter 13 (41), 7644–7648. https://doi.org/10.1039/C7SM01417A.

Lee, J., Lee, K.Y., 2009. Local and sustained vascular endothelial growth factor delivery for angiogenesis using an injectable system. Pharm. Res. 26 (7), 1739–1744. https://doi.org/10.1007/s11095-009-9884-4.

Lee, K.Y., Mooney, D.J., 2012. Alginate: Properties and biomedical applications. Prog. Polym. Sci. 37 (1), 106–126. https://doi.org/10.1016/j.progpolymsci.2011.06.003.

Lekka, M., Sainz-Serp, D., Kulik, A.J., Wandrey, C., 2004. Hydrogel microspheres: Influence of chemical composition on surface morphology, local elastic properties, and bulk mechanical characteristics. Langmuir 20, 9968–9977. https://doi.org/10.1021/la048389h.

LeRoux, M.A., Guilak, F., Setton, L.A., 1999. Compressive and shear properties of alginate gel: Effects of sodium ions and alginate concentration. J. Biomed. Mater. Res. https://doi.org/10.1002/(SICI)1097-4636(199910)47:1<46::AID-JBM6>3.0.CO;2-N.

Li, X., Huang, Q., Elkhooly, T.A., Liu, Y., Wu, H., Feng, Q., Liu, L., Fang, Y.u., Zhu, W., Hu, T., 2018. Effects of titanium surface roughness on the mediation of osteogenesis via modulating the immune response of macrophages. Biomed. Mater. 13 (4), 045013. https://doi.org/10.1088/1748-605X/aabe33.

Lim, F., Sun, A., 1980. Microencapsulated islets as bioartificial endocrine pancreas. Science (80-. 210 (4472), 908–910. https://doi.org/10.1126/science:6776628.

Makkar, R.R., Smith, R.R., Cheng, K., Malliaras, K., Thomson, L.E.J., Berman, D., Czer, L.S.C., Marbán, L., Mendizabal, A., Johnston, P.V., Russell, S.D., Schuleri, K.H., Lardo, A.C., Gerstenblith, G., Marbán, E., 2012. Intracoronary cardiosphere-derived cells for heart regeneration after myocardial infarction (CADUCEUS): A prospective, randomised phase 1 trial. Lancet 379 (9819), 895–904. https://doi.org/10.1016/S0140-6736(12)60195-0.

Malpique, R., Osório, L.M., Ferreira, D.S., Ehrhart, F., Brito, C., Zimmermann, H., Alves, P.M., 2010. Alginate encapsulation as a novel strategy for the cryopreservation of neurospheres. Tissue Eng. - Part C Methods. 16 (5), 965–977. https://doi.org/10.1089/ten.tec.2009.0660.

Mason, B.N., Starchenko, A., Williams, R.M., Bonassar, L.J., Reinhart-King, C.A., 2013. Tuning three-dimensional collagen matrix stiffness independently of collagen concentration modulates endothelial cell behavior. Acta Biomater 9 (1), 4635–4644. https://doi.org/10.1016/j.actbio.2012.08.007.

Matsumoto, Y., Morinaga, Y., Ujihira, M., Oka, K., Tanishita, K., 2001. Improvement in the viability of cryopreserved cells by microencapsulation. JSME Int. Journal, Ser. C Mech. Syst. Mach. Elem. Manuf. 44 (4), 937–945. https://doi.org/10.1299/jsmec.44.937.

Moya, M.L., Morley, M., Khanna, O., Opara, E.C., Brey, E.M., 2012. Stability of alginate microbead properties in vitro. J. Mater. Sci. Mater. Med. 23 (4), 903–912. https://doi.org/10.1007/s10856-012-4575-9.

Nečas, D., Klapetek, P., 2012. Gwyddion: An open-source software for SPM data analysis. Cent. Eur. J. Phys. https://doi.org/10.2478/s11534-011-0096-2.

Neubauer, M.P., Poehlmann, M., Fery, A., 2014. Microcapsule mechanics: From stability to function. Adv. Colloid Interface Sci. 207, 65–80. https://doi.org/10.1016/j.cis.2013.11.016.

Orive, G., Hernández, R.M., Gascón, A.R., Igartua, M., Pedraz, J.L., 2003. Survival of different cell lines in alginate-agarose microcapsules. Eur. J. Pharm. Sci. 18 (1), 23–30. https://doi.org/10.1016/S0928-0987(02)00220-8.

Orive, G., Maria Hernández, R., Rodríguez Gascón, A., Calafiore, R., Swi Chang, T.M., Vos, P.d., Hortelano, G., Hunkeler, D., Lacík, I., Luis Pedraz, J., 2004. History, challenges and perspectives of cell microencapsulation. Trends Biotechnol 22 (2), 87–92. https://doi.org/10.1016/j.tibtech.2003.11.004.

Orive, G., Ponce, S., Hernández, R.M., Gascón, A.R., Igartua, M., Pedraz, J.L., 2002. Biocompatibility of microcapsules for cell immobilization elaborated with different type of alginates. Biomaterials 23 (18), 3825–3831. https://doi.org/10.1016/S0142-9612(02)00118-7.

Paul, A., Ge, Y., Prakash, S., Shum-Tim, D., 2009. Microencapsulated stem cells for tissue repairing: Implications in cell-based myocardial therapy. Regen. Med. https://doi.org/10.2217/rme.09.43.

Petersen, A., Joly, P., Bergmann, C., Korus, G., Duda, G.N., 2012. The impact of substrate stiffness and mechanical loading on fibroblast-induced scaffold remodeling. Tissue Eng. - Part A. https://doi.org/10.1089/ten.tea.2011.0514.

Petrochenko, P.E., Kumar, G., Fu, W., Zhang, Q., Zheng, J., Liang, C., Goering, P.L., Narayan, R.J., 2015. Nanoporous aluminum oxide membranes coated with atomic layer deposition-grown titanium dioxide for biomedical applications: An in vitro evaluation. J. Biomed. Nanotechnol. 11, 2275–2285. https://doi.org/10.1166/jbn.2015.2169.

Rokstad, A.M.A., Lacík, I., de Vos, P., Strand, B.L., 2014. Advances in biocompatibility and physico-chemical characterization of microspheres for cell encapsulation. Adv. Drug Deliv. Rev. https://doi.org/10.1016/j.addr.2013.07.010.

Sarrazin, B., Tsapis, N., Mousnier, L., Taulier, N., Urbach, W., Guenoun, P., 2016. AFM investigation of liquid-filled polymer microcapsules elasticity. Langmuir. https://doi.org/10.1021/acs.langmuir.6b00431.

Sasikumar, S., Chameettachal, S., Cromer, B., Pati, F., Kingshott, P., 2019. Decellularized extracellular matrix hydrogels—cell behavior as a function of matrix stiffness. Curr. Opin. Biomed. Eng. 10, 123–133. https://doi.org/10.1016/j.cobme.2019.05.002.

Tompkins, B.A., Balkan, W., Winkler, J., Gyöngyösi, M., Goliasch, G., Fernández-Avilés, F., Hare, J.M., 2018. Preclinical Studies of Stem Cell Therapy for Heart Disease. Circ. Res. 122, 1006–1020. https://doi.org/10.1161/CIRCRESAHA.117.312486.

Van Ramshorst, J., Rodrigo, S.F., Schalij, M.J., Beeres, S.L.M.A., Bax, J.J., Atsma, D.E., 2011. Bone marrow cell injection for chronic myocardial ischemia: The past and the future. J. Cardiovasc. Transl. Res. https://doi.org/10.1007/s12265-010-9249-8.

Virumbrales-Muñoz, M., Paz-Artigas, L., Ciriza, J., Alcaine, C., Espona-Noguera, A., Doblaré, M., Sáenz del Burgo, L., Ziani, K., Pedraz, J.L., Fernández, L., Ochoa, I., 2021. Force Spectroscopy Imaging and Constriction Assays Reveal the Effects of Graphene Oxide on the Mechanical Properties of Alginate Microcapsules. ACS Biomater. Sci. Eng. 7 (1), 242–253. https://doi.org/10.1021/acsbiomaterials.0c01382.s002.

Virumbrales-Muñoz, M., Santos-Vizcaino, E., Paz, L., Gallardo-Moreno, A.M., Orive, G., Hernandez, R.M., Doblaré, M., Gonzalez-Martin, M.L., Fernández, L.J., Pedraz, J.L., Ochoa, I., 2019. Force spectroscopy-based simultaneous topographical and mechanical characterization to study polymer-to-polymer interactions in coated alginate microspheres. Sci. Rep. https://doi.org/10.1038/s41598-019-56547-z.

Xu, Y., Patnaik, S., Guo, X., Li, Z., Lo, W., Butler, R., Claude, A., Liu, Z., Zhang, G., Liao, J., Anderson, P.M., Guan, J., 2014. Cardiac differentiation of cardiosphere-derived cells in scaffolds mimicking morphology of the cardiac extracellular matrix. Acta Biomater. https://doi.org/10.1016/j.actbio.2014.04.018.

Yee, K., Malliaras, K., Kanazawa, H., Tseliou, E., Cheng, K., Luthringer, D.J., Ho, C.S., Takayama, K., Minamino, N., Dawkins, J.F., Chowdhury, S., Duong, D.T., Seinfeld, J., Middleton, R.C., Dharmakumar, R., Li, D., Marbán, L., Makkar, R.R., Marbán, E., 2014. Allogeneic cardiospheres delivered via percutaneous transendocardial injection increase viable myocardium, decrease scar size, and attenuate cardiac dilatation in porcine ischemic cardiomyopathy. PLoS One 9, e113805. https://doi.org/10.1371/journal.pone.0113805.

Ziani, K., Espona-Noguera, A., Crisóstomo, V., Casado, J.G., Sanchez-Margallo, F.M., Saenz-del-Burgo, L., Ciriza, J., Pedraz, J.L., 2021. Characterization of encapsulated porcine cardiosphere-derived cells embedded in 3D alginate matrices. Int. J. Pharm. 599, 120454. https://doi.org/10.1016/j.ijpharm.2021.120454.

Zimmermann, H., Shirley, S.G., Zimmermann, U., 2007. Alginate-based encapsulation of cells: Past, present, and future. Current Diabetes Reports 7 (4), 314–320. https://doi.org/10.1007/s11892-007-0051-1.